

# Impact of chemical potential on the reflectance of graphene in the infrared and microwave domains

G. L. Klimchitskaya,<sup>1,2</sup> V. M. Mostepanenko,<sup>1,2,3</sup> and V. M. Petrov<sup>4</sup>

<sup>1</sup>*Central Astronomical Observatory at Pulkovo of the Russian Academy of Sciences, Saint Petersburg, 196140, Russia*

<sup>2</sup>*Institute of Physics, Nanotechnology and Telecommunications, Peter the Great Saint Petersburg Polytechnic University, Saint Petersburg, 195251, Russia*

<sup>3</sup>*Kazan Federal University, Kazan, 420008, Russia*

<sup>4</sup>*Institute of Advanced Manufacturing Technologies, Peter the Great Saint Petersburg Polytechnic University, Saint Petersburg, 195251, Russia*

## Abstract

The reflectance of graphene is investigated in the framework of the Dirac model with account of its realistic properties, such as nonzero chemical potential and band gap, at any temperature. For this purpose, the exact reflection coefficients of the electromagnetic waves on a graphene sheet expressed via the polarization tensor and ultimately via the electrical conductivity of graphene have been used. The reflectance of graphene is computed as a function of frequency and chemical potential at different temperatures and values of the band-gap parameter. The minimum values of the reflectance are found which are reached in the infrared domain at the points of vanishing imaginary part of the conductivity of graphene. For a gapped graphene, the maximum reflectance equal to unity is reached at the points where the imaginary part of conductivity diverges. The computational results demonstrate an interesting interplay between the band gap and chemical potential in their combined effect on the reflectance. Specifically, there are wide frequency intervals where the reflectance of graphene increases with increasing chemical potential and decreasing band gap. The numerical computations are found to be in good agreement with the analytic asymptotic expressions in the regions of their applicability. Several technological areas, where the obtained results could be used, are listed.

## I. INTRODUCTION

Currently the reflectivity properties of graphene have been investigated both theoretically and experimentally using a variety of approaches and techniques [1, 2]. In the majority of cases, studies on the optics of graphene were based on the investigation of its electrical conductivity. On this subject a great number of results have been obtained using the Kubo formalism, the Boltzmann transport theory, the current-current correlation functions, the two-dimensional Drude model, and others (see the review papers [3–5]). Although some of these approaches employ simple intuitive models and are of phenomenological character, they were fruitfully used to investigate the reflectivity of graphene in different spectral domains [6–13]. In addition to the academic interest, a knowledge of the reflectivity properties is required in prospective technological applications of graphene, such as in the modulators, detectors and switches [11, 13, 14], solar cells [15], corrosion protection [16], transparent electrodes [17] etc.

A more complete theory of the optical properties of graphene at relatively low frequencies in the microwave and infrared domains would be beneficial for both fundamental physics and its applications. Fortunately, at these frequencies (i.e., at energies below 1–2 eV) graphene is well described by the Dirac model. This model assumes that graphene quasiparticles are massless or very light and obey the (2+1)-dimensional Dirac equation, where the Fermi velocity  $v_F = c/300$  plays the role of the speed of light  $c$  [1, 2, 18]. In the framework of the Dirac model, it is possible to obtain an exact expression for the polarization tensor of graphene on the basis of first principles of quantum electrodynamics at nonzero temperature. This tensor describes a response of graphene to the electromagnetic field and, thus, can be used for a unified theoretical description of the broad range of physical phenomena including the Casimir and van der Waals forces, electrical conductivity and optical properties. Taking into account that the Dirac model incorporates naturally a nonzero band gap  $\Delta$  in the energy spectrum of quasiparticles and a chemical potential  $\mu$ , the polarization tensor provides the reliable foundation for a description of physical processes in real (doped) graphene samples at energies below 1–2 eV. At higher energies, i.e., beyond the Dirac model, the conductivity and reflectivity properties of the graphene-like materials have been studied with account of Coulomb interaction, interactions with phonons, and a magnetic field [2, 7, 18–24].

The exact expression for the polarization tensor of graphene at zero temperature in the

one-loop approximation was derived in Ref. [25] (see also Ref. [26] and literature therein for some special cases considered previously). In Ref. [27] the polarization tensor at nonzero temperature has been found, but only at the pure imaginary Matsubara frequencies. The polarization tensor of Ref. [27] was used to derive the Lifshitz-type formula, where the reflection coefficients are expressed via this tensor, and to investigate the fluctuation-induced van der Waals and Casimir forces in graphene systems [27–38]. It was not possible, however, to calculate the electrical conductivity and optical properties of graphene which are expressed via the polarization tensor defined at real frequencies. Another representation for the polarization tensor of graphene at nonzero temperature, allowing an analytic continuation to the entire complex frequency plane, was found in Ref. [39]. It is significant that at the pure imaginary Matsubara frequencies the representations of Refs. [27] and [39] coincide, but take dissimilar values at all other frequencies. A more universal representation of Ref. [39] was used in calculations of the Casimir force [40–43] and, after a continuation to the axis of real frequencies, for investigation of the electrical conductivity [44, 45] and reflectances [46–48] of an undoped graphene.

The polarization tensor of doped graphene with a nonzero chemical potential has been derived in Ref. [49] using the representation of Ref. [39]. This tensor was used to study an impact of nonzero chemical potential on the thermal Casimir force in graphene systems Refs. [50, 51] and, after a continuation to the axis of real frequencies, on the electrical conductivity of graphene [52]. As a result, the theory of electrical conductivity of graphene has been developed in the framework of the Dirac model, which takes into a complete account the effect of the nonzero band gap and chemical potential. The derived expressions for real and imaginary parts of the conductivity of graphene were found to be in agreement with the causality conditions and satisfy the Kramers-Kronig relations [53]. This solved the problem which was under a discussion in the previous literature [54–57].

In this paper, the recently developed theory is applied to investigate an impact of chemical potential on the reflectance of gapped graphene in the application region of the Dirac model, i.e., in the infrared and microwave domains. We present the exact reflection coefficients and reflectance for the transverse magnetic and transverse electric (i.e.,  $p$ - and  $s$ -polarized) electromagnetic waves on a graphene sheet expressed via the polarization tensor or via the conductivity. An explicit expression for the angular dependence of graphene reflectance, giving the major contribution to the results, is also obtained. The reflectance of graphene

at the normal incidence is investigated as a function of frequency and chemical potential at different temperatures  $T$  and values of the band-gap parameter. It is shown that the minimum reflectance is reached at the values of frequency and chemical potential where the imaginary part of the conductivity of graphene vanishes. In doing so, the minimum reflectance either vanishes or takes rather small value depending on the magnitude of the real part of conductivity. At different temperatures a qualitatively different impact of the chemical potential on the reflectance of graphene is observed. The computational results demonstrate an interesting interplay between the band gap and chemical potential in their combined effect on the reflectance. There are rather wide frequency intervals where the reflectance increases with increasing chemical potential and decreasing band gap.

The paper is organized as follows. In Sec. II, we present general expressions for the reflectance of graphene in the framework of the Dirac model in the case of nonzero band gap and chemical potential. In Sec. III, the impact of chemical potential on the reflectance is investigated for a gapless graphene. Section IV is devoted to an interplay in the impact of nonzero band gap and chemical potential of graphene on its reflectance. In Sec. V, the reader will find our conclusions and discussion.

## II. REFLECTANCE OF GRAPHENE IN THE FRAMEWORK OF THE DIRAC MODEL

We consider a plane wave of frequency  $\omega$  incident on the graphene sheet under the angle  $\theta_i$ . For real photons on a mass shell the magnitude of the wave-vector component parallel to graphene is  $k = \omega \sin \theta_i / c$ . Then the amplitude reflection coefficients for the transverse magnetic (TM) and transverse electric (TE) polarizations of the electromagnetic field along the real frequency axis are given by [39, 47]

$$\begin{aligned} r_{\text{TM}}(\omega, \theta_i) &= \frac{\omega \cos \theta_i \Pi_{00}(\omega, k)}{2i\hbar ck^2 + \omega \cos \theta_i \Pi_{00}(\omega, k)}, \\ r_{\text{TE}}(\omega, \theta_i) &= \frac{c\Pi(\omega, k)}{2i\hbar\omega k^2 \cos \theta_i - c\Pi(\omega, k)}. \end{aligned} \quad (1)$$

Here,  $\Pi_{00}$  is the 00 component of the polarization tensor of graphene  $\Pi_{\mu\nu}$ ,  $\mu, \nu = 0, 1, 2$  and

$$\Pi(\omega, k) = k^2 \Pi_{\text{tr}}(\omega, k) + \left( \frac{\omega^2}{c^2} - k^2 \right) \Pi_{00}(\omega, k), \quad (2)$$

where  $\Pi_{\text{tr}} \equiv \Pi_{\mu}^{\mu}$  is the trace of this tensor. Note that in calculations of the Casimir force between two graphene sheets one should replace  $\omega$  in Eq. (1) with the pure imaginary Matsubara frequencies  $i\xi_l = 2\pi i k_B T l / \hbar$ , where  $k_B$  is the Boltzmann constant and  $l = 0, 1, 2, \dots$ , and consider  $\omega$  and  $k$  as independent quantities (see Refs. [27–38, 40–43] for details). When calculating the van der Waals (Casimir-Polder) forces between separate atoms, the role of polarization tensor is played by the atomic dynamic polarizabilities [58].

It is well known that the polarization tensor is closely related to the in-plane and out-of-plane nonlocal conductivities of graphene [37, 44, 45, 47, 52]

$$\begin{aligned}\sigma_{\parallel}(\omega, k) &= -i \frac{\omega}{4\pi \hbar k^2} \Pi_{00}(\omega, k), \\ \sigma_{\perp}(\omega, k) &= i \frac{c^2}{4\pi \hbar \omega k^2} \Pi(\omega, k).\end{aligned}\quad (3)$$

Substituting Eq. (3) in Eq. (1), we express the reflection coefficients on a graphene sheet in terms of its conductivities

$$\begin{aligned}r_{\text{TM}}(\omega, \theta_i) &= \frac{2\pi \cos \theta_i \sigma_{\parallel}(\omega, k)}{c + 2\pi \cos \theta_i \sigma_{\parallel}(\omega, k)}, \\ r_{\text{TE}}(\omega, \theta_i) &= -\frac{2\pi \sigma_{\perp}(\omega, k)}{c \cos \theta_i + 2\pi \sigma_{\perp}(\omega, k)}.\end{aligned}\quad (4)$$

The reflectances of graphene for two independent polarizations of the electromagnetic field are defined as

$$\mathcal{R}_{\text{TM(TE)}}(\omega, \theta_i) = |r_{\text{TM(TE)}}(\omega, \theta_i)|^2. \quad (5)$$

Taking into account that both the polarization tensor and the conductivities of graphene are the complex quantities, from Eqs. (4) and (5) one obtains

$$\begin{aligned}\mathcal{R}_{\text{TM}}(\omega, \theta_i) &= \frac{4\pi^2 \cos^2 \theta_i [\text{Re}^2 \sigma_{\parallel}(\omega, k) + \text{Im}^2 \sigma_{\parallel}(\omega, k)]}{[c + 2\pi \cos \theta_i \text{Re} \sigma_{\parallel}(\omega, k)]^2 + 4\pi^2 \cos^2 \theta_i \text{Im}^2 \sigma_{\parallel}(\omega, k)}, \\ \mathcal{R}_{\text{TE}}(\omega, \theta_i) &= \frac{4\pi^2 [\text{Re}^2 \sigma_{\perp}(\omega, k) + \text{Im}^2 \sigma_{\perp}(\omega, k)]}{[c \cos \theta_i + 2\pi \text{Re} \sigma_{\perp}(\omega, k)]^2 + 4\pi^2 \text{Im}^2 \sigma_{\perp}(\omega, k)}\end{aligned}\quad (6)$$

These equations take especially simple form in the case of normal incidence  $\theta_i = k = 0$

$$\mathcal{R}(\omega) = \mathcal{R}_{\text{TM}}(\omega, 0) = \mathcal{R}_{\text{TE}}(\omega, 0) = \frac{4\pi^2 [\text{Re}^2 \sigma(\omega) + \text{Im}^2 \sigma(\omega)]}{[c + 2\pi \text{Re} \sigma(\omega)]^2 + 4\pi^2 \text{Im}^2 \sigma(\omega)}, \quad (7)$$

where  $\sigma(\omega) \equiv \sigma_{\parallel}(\omega, 0) = \sigma_{\perp}(\omega, 0)$  is the conductivity of graphene in the local limit. In the framework of the Dirac model, this conductivity was found [52] using Eq. (3) and exact

expressions for the polarization tensor of graphene with arbitrary band gap  $\Delta$  and chemical potential  $\mu$  at any temperature  $T$ . This opens the way for a sophisticated treatment of the reflectance of graphene (6) and (7) over the entire application region of the Dirac model, i.e., at all frequencies below 1–2 eV.

We begin with a brief summary of the exact results for  $\sigma(\omega)$  at arbitrary values of  $T$ ,  $\Delta$ , and  $\mu$  [52]. The real part of the local conductivity is given by

$$\begin{aligned} \text{Re}\sigma(\omega) &= \sigma_0 \theta(\hbar\omega - \Delta) \frac{(\hbar\omega)^2 + \Delta^2}{2(\hbar\omega)^2} \\ &\times \left( \tanh \frac{\hbar\omega + 2\mu}{4k_B T} + \tanh \frac{\hbar\omega - 2\mu}{4k_B T} \right), \end{aligned} \quad (8)$$

where the universal conductivity  $\sigma_0 = e^2/(4\hbar)$ ,  $\theta(x)$  is the step function equal to unity for  $x \geq 0$  and to zero for  $x < 0$ . Note that Eq. (8) is interpreted as originating from the interband transitions [8]. At moderate frequencies satisfying the condition  $\Delta \leq \hbar\omega \ll 2\mu$  the following asymptotic expression is valid:

$$\text{Re}\sigma(\omega) = \sigma_0 \frac{(\hbar\omega)^2 + \Delta^2}{(\hbar\omega)^2} \frac{\hbar\omega}{4k_B T} \text{sech}^2 \frac{\mu}{2k_B T}. \quad (9)$$

The exact expression for the imaginary part of the local conductivity of graphene takes the form [52]

$$\text{Im}\sigma(\omega) = \frac{\sigma_0}{\pi} \left[ \frac{2\Delta}{\hbar\omega} - \frac{(\hbar\omega)^2 + \Delta^2}{(\hbar\omega)^2} \ln \left| \frac{\hbar\omega + \Delta}{\hbar\omega - \Delta} \right| + Y(\omega) \right], \quad (10)$$

where

$$\begin{aligned} Y(\omega) &= 2 \int_{\Delta/(\hbar\omega)}^{\infty} dt \sum_{\kappa=\pm 1} \frac{1}{e^{\frac{\hbar\omega t + 2\kappa\mu}{2k_B T}} + 1} \\ &\times \left[ 1 + \frac{(\hbar\omega)^2 + \Delta^2}{(\hbar\omega)^2} \frac{1}{t^2 - 1} \right]. \end{aligned} \quad (11)$$

Under the conditions  $k_B T \ll \mu$ ,  $\Delta < 2\mu$ , and  $\hbar\omega \ll 2\mu$  Eqs. (10) and (11) lead to the simple asymptotic result

$$\text{Im}\sigma(\omega) = \frac{\sigma_0}{\pi} \left[ \frac{4\mu}{\hbar\omega} - 4 \ln 2 \frac{k_B T}{\hbar\omega} - \frac{(\hbar\omega)^2 + \Delta^2}{(\hbar\omega)^2} \ln \frac{2\mu + \hbar\omega}{2\mu - \hbar\omega} \right]. \quad (12)$$

The first Drude-like term on the right-hand side of this equation was interpreted as originating from the intraband transitions [6].

If, however,  $k_B T \ll \mu$ , but  $\Delta > 2\mu$  one finds

$$\begin{aligned} \text{Im}\sigma(\omega) &= \frac{\sigma_0}{\pi} \left[ \frac{2\Delta}{\hbar\omega} + 16 \frac{\Delta^2}{\Delta^2 - (\hbar\omega)^2} \frac{k_B T}{\hbar\omega} e^{-\frac{\Delta}{2k_B T}} \cosh \frac{\mu}{k_B T} \right. \\ &\left. - \frac{(\hbar\omega)^2 + \Delta^2}{(\hbar\omega)^2} \ln \left| \frac{\hbar\omega + \Delta}{\hbar\omega - \Delta} \right| \right]. \end{aligned} \quad (13)$$

This asymptotic expression is applicable at any frequency. Note that Ref. [52], where Eq. (13) was obtained, contains two typos, i.e., indicates an incorrect factor  $8 \ln 2$  instead of 16 and  $k_B T$  instead of  $2k_B T$  in the power of an exponent.

In the end of this section we note that a knowledge of the exact expressions (8) and (10) for the local conductivity of graphene  $\sigma(\omega)$  enables one to obtain the highly accurate approximate values for the TM and TE reflectances at the arbitrary angle of incidence. To do so, we represent the nonlocal in-plane and out-of-plane conductivities of graphene in the form [52]

$$\begin{aligned}\sigma_{\parallel}(\omega, k) &= \sigma(\omega) + O\left(\frac{v_F^2}{c^2}\right), \\ \sigma_{\perp}(\omega, k) &= \sigma(\omega) + O\left(\frac{v_F^2}{c^2}\right),\end{aligned}\tag{14}$$

where the nonlocal corrections to local results are of the order of  $10^{-5}$ . Substituting Eq. (14) in Eq. (6), we obtain

$$\begin{aligned}\mathcal{R}_{\text{TM}}(\omega, \theta_i) &= \frac{4\pi^2 \cos^2 \theta_i [\text{Re}^2 \sigma(\omega) + \text{Im}^2 \sigma(\omega)]}{[c + 2\pi \cos \theta_i \text{Re} \sigma(\omega)]^2 + 4\pi^2 \cos^2 \theta_i \text{Im}^2 \sigma(\omega)} + O\left(\frac{v_F^2}{c^2}\right), \\ \mathcal{R}_{\text{TE}}(\omega, \theta_i) &= \frac{4\pi^2 [\text{Re}^2 \sigma(\omega) + \text{Im}^2 \sigma(\omega)]}{[c \cos \theta_i + 2\pi \text{Re} \sigma(\omega)]^2 + 4\pi^2 \text{Im}^2 \sigma(\omega)} + O\left(\frac{v_F^2}{c^2}\right).\end{aligned}\tag{15}$$

This result is applicable with exception of only extremely narrow vicinities of frequencies  $\omega_k$ , where  $\text{Re}\sigma(\omega_k) = \text{Im}\sigma(\omega_k) = 0$  holds (see Sec. IV for a few examples). At all other frequencies Eq. (15) provides an explicit angular dependence of the reflectances of graphene already discussed previously in Refs. [39, 46]. Because of this, below we mostly concentrate on the impact of chemical potential on the reflectance of graphene at the normal incidence. Note also that in calculations of the van der Waals and Casimir forces one should take into account the dependence of the conductivity of graphene on both  $\omega$  and  $k$ . This is because in the Lifshitz theory they are not constrained by the mass shell equation.

### III. IMPACT OF CHEMICAL POTENTIAL IN THE CASE OF GAPLESS GRAPHENE

We consider the reflectance of graphene with  $\Delta = 0$  at the normal incidence given by Eq. (7). The real and imaginary parts of conductivity are presented in Eqs. (8), (10), and (11) where one should put  $\Delta = 0$ . Using these equations, we first computed the reflectance

of graphene  $\mathcal{R}$  at  $T = 300$  K as a function of frequency in the frequency region from  $2 \times 10^{-5}$  to 1 eV belonging to the microwave and infrared domains. The computational results are presented in Fig. 1 by the lines 1, 2, and 3 plotted for the chemical potential  $\mu$  equal to 0.02, 0.1, and 0.2 eV, respectively.

As is seen in Fig. 1, the reflectance of graphene reaches the minimum value at the frequencies  $\hbar\omega_m = 0.068, 0.16,$  and  $0.32$  eV for the lines 1, 2, and 3, respectively. With increasing  $\mu$ , the minimum of  $\mathcal{R}$  becomes more pronounced. Note also that at all frequencies  $\text{Re}\sigma \neq 0$  and strongly depends on both  $\omega$  and  $\mu$ . In so doing we have  $2\mu < \hbar\omega_m < \hbar\omega_0$  where  $\omega_0$  is the root of the imaginary part of conductivity  $\text{Im}\sigma(\omega_0) = 0$ . For the lines labeled 2 and 3  $\hbar\omega_m < 2\mu$  and  $\omega_m \approx \omega_0$  hold. An impact of the chemical potential on  $\mathcal{R}$  is rather strong only within the frequency interval from  $2 \times 10^{-4}$  to 0.6 eV which mostly belongs to the infrared domain. For  $\hbar\omega < 0.1$  eV the reflectance is larger for graphene with smaller chemical potential.

Next, we consider the dependence of  $\mathcal{R}$  on the frequency at lower temperatures. In Fig. 2(a), the lines 1, 2, and 3 show the computational results at the liquid nitrogen temperature  $T = 77$  K for the chemical potential  $\mu$  equal to 0.02, 0.1, and 0.2 eV, respectively. As is seen in Fig. 2(a), the minimum values of the reflectance are reached at  $\hbar\omega_m = 0.034, 0.16,$  and  $0.33$  eV for the lines 1, 2, and 3, respectively. Thus, in comparison with Fig. 1 plotted at  $T = 300$  K, the position of the first minimum is shifted to lower frequencies. For all the three lines the inequality  $\hbar\omega_m < 2\mu$  holds and  $\omega_m \approx \omega_0$ .

Similar results, but at the liquid helium temperature  $T = 4.4$  K, are presented in Fig. 2(b). Here,  $\hbar\omega_m = 0.034, 0.165,$  and  $0.335$  eV and, again,  $\hbar\omega_m < 2\mu$  and  $\omega_m \approx \omega_0$  for all the three lines. Note that for the lines 2 and 3 the minimum values of  $\mathcal{R}$  equal to  $10^{-10}$  and  $< 10^{-17}$  cannot be shown in the used scale of Fig. 2(b). So small minimum values of  $\mathcal{R}$  are caused by the fact that at very low temperatures under the condition  $\hbar\omega < 2\mu$  the real part of conductivity becomes negligibly small (at  $T = 0$  and  $\hbar\omega < 2\mu$  the exact equality  $\text{Re}\sigma = 0$  is valid [52]). The distinctive feature of Fig. 2(b), as compared to Figs. 1 and 2(a), is the presence of small peaks at  $\hbar\omega = 2\mu$  just after the points of each minimum of  $\mathcal{R}$ . These peaks arise for the reason that at zero temperature  $\text{Im}\sigma \rightarrow \infty$  when  $\hbar\omega \rightarrow 2\mu$  resulting in an unphysically narrow maximum  $\mathcal{R} = 1$  [52].

For a gapless graphene under consideration in this section, the behavior of its reflectance at sufficiently small  $\omega$  can be found analytically. For this purpose we consider first the

imaginary part of conductivity. From Eqs. (10) and (11) one obtains

$$\begin{aligned} \text{Im}\sigma(\omega) &= \frac{2\sigma_0}{\pi} \int_0^\infty dt \sum_{\kappa=\pm 1} \frac{1}{e^{\frac{\hbar\omega t + 2\kappa\mu}{2k_B T}} + 1} \\ &\quad \times \left(1 + \frac{1}{t^2 - 1}\right). \end{aligned} \quad (16)$$

It is convenient to introduce the new integration variable  $u = \hbar\omega t/(2k_B T)$  in the first contribution on the right-hand side of Eq. (16), which is associated with unity in the brackets, and leave the second contribution as is

$$\begin{aligned} \text{Im}\sigma(\omega) &= \frac{4k_B T \sigma_0}{\pi \hbar \omega} \int_0^\infty du \left( \frac{e^{-\frac{\mu}{k_B T}}}{e^u + e^{-\frac{\mu}{k_B T}}} + \frac{e^{\frac{\mu}{k_B T}}}{e^u + e^{\frac{\mu}{k_B T}}} \right) \\ &\quad + \frac{2\sigma_0}{\pi} \int_0^\infty \frac{dt}{t^2 - 1} \sum_{\kappa=\pm 1} \frac{1}{e^{\frac{\hbar\omega t + 2\kappa\mu}{2k_B T}} + 1}. \end{aligned} \quad (17)$$

The first contribution on the right-hand side of Eq. (17) has the first-order pole at  $\omega = 0$  whereas the second contribution converges in the sense of the principal value. At  $\omega = 0$  the second contribution is proportional to

$$\int_0^\infty \frac{dt}{t^2 - 1} = 0. \quad (18)$$

Because of this, one can neglect by the second contribution on the right-hand side of Eq. (17), as compared to the first one. Integrating the first contribution with respect to  $u$ , we arrive at

$$\begin{aligned} \text{Im}\sigma(\omega) &\approx \frac{4k_B T \sigma_0}{\pi \hbar \omega} \left[ \ln \left(1 + e^{-\frac{\mu}{k_B T}}\right) + \ln \left(1 + e^{\frac{\mu}{k_B T}}\right) \right] \\ &= \frac{8k_B T \sigma_0}{\pi \hbar \omega} \ln \left(2 \cosh \frac{\mu}{2k_B T}\right). \end{aligned} \quad (19)$$

Now we take into account that in accordance with Eq. (8)  $\text{Re}\sigma$  goes to zero with vanishing frequency (we recall that  $\Delta = 0$  in this case). Then, for sufficiently small frequencies satisfying the condition

$$\hbar\omega \ll 8k_B T \ln \left(2 \cosh \frac{\mu}{2k_B T}\right), \quad (20)$$

we obtain from Eqs. (7) and (19)

$$\begin{aligned} \mathcal{R} &\approx 1 - \left[ \frac{c}{2\pi \text{Im}\sigma(\omega)} \right]^2 \\ &= 1 - \left[ \frac{\hbar\omega}{4\alpha k_B T \ln \left(2 \cosh \frac{\mu}{2k_B T}\right)} \right]^2. \end{aligned} \quad (21)$$

Here,  $\alpha = e^2/(\hbar c)$  is the fine structure constant.

To find the application region of the asymptotic expression (21), we have compared the results of analytic calculations using this expression with the computational results presented in Figs. 1 and 2. Thus, for the lines 1, 2, and 3 presented in Fig. 1 ( $T = 300$  K) the analytic results are in agreement with the numerical ones within 1% at all frequencies below 0.15, 0.5, and 1 meV, respectively. The application region of Eq. (21) only slightly depends on the value of temperature. Thus, for the lines 1, 2, and 3 in Fig. 2(a) ( $T = 77$  K) the analytic results agree with the numerical ones at smaller than 0.1, 0.5, and 0.9 meV frequencies, respectively. At  $T = 4.4$  K the region of applicability of Eq. (21) is almost unchanged.

We continue with the case of gapless graphene and compute the reflectance given by Eqs. (7), (8), (10), and (11) as a function of chemical potential at different temperatures. The computational results at  $\hbar\omega = 0.01$  eV are presented in Fig. 3 by the lines 1, 2, and 3 at  $T = 300, 77,$  and  $4.4$  K, respectively, for the values of  $\mu$  varying from 0 to 0.2 eV. As is seen in this figure, on the condition that  $\mu < \hbar\omega/2 = 0.005$  eV the reflectance of graphene is almost independent on the chemical potential. For  $\mu > 0.07$  eV the computational results become nearly independent on the temperature. For the lines 1 and 2 the smallest value of  $\mathcal{R}$  is reached at  $\mu = 0$ . At the liquid helium temperature (the line 3) the minimum value of  $\mathcal{R}$  is reached at  $\mu = 0.006$  eV, i.e., under a condition  $\hbar\omega < 2\mu$  [see the discussion related to Fig. 2(b)].

As a next step, we compute the reflectance of graphene as a function of the chemical potential at higher frequency  $\hbar\omega = 0.2$  eV. The computational results are presented in Fig. 4(a) by the lines 1, 2, and 3 at  $T = 300, 77,$  and  $4.4$  K, respectively. In Fig. 4(b) a vicinity of the points of minimum reflectance is shown on an enlarged scale for better visualization. From Fig. 4(a) it is seen that for  $\mu < 0.05$  eV the reflectance of graphene is nearly independent on  $\mu$ . The minimum values of the reflectance are reached at  $\mu = 0.13, 0.128,$  and  $0.12$  eV for the lines 1, 2, and 3, respectively. In all these cases the condition  $\hbar\omega < 2\mu$  holds. This explains why the minimum value becomes smaller with decreasing temperature. At  $T = 4.4$  K the minimum value of  $\mathcal{R}$  is equal to  $3 \times 10^{-11}$ . The nature of a peak in Figs. 4(a) and 4(b) arising on the line 3 ( $T = 4.4$  K) under the condition  $2\mu = \hbar\omega$ , i.e., at  $\mu = 0.1$  eV, is the same as was discussed in relation to Fig. 2(b). It arises because at zero temperature the imaginary part of conductivity turns to infinity when  $2\mu = \hbar\omega$  resulting in  $\mathcal{R} = 1$ . Note also that for  $\hbar\omega = 0.2$  eV the reflectance becomes temperature-independent

at  $\mu > 0.18$  eV.

#### IV. INTERPLAY BETWEEN NONZERO BAND GAP AND CHEMICAL POTENTIAL

In this section, we consider the reflectance of graphene in the most general case of nonzero temperature, band gap and chemical potential. The numerical computations are performed using Eqs. (7), (8), (10), and (11). The computational results for the reflectance as a function of frequency at  $T = 300$  K,  $\mu = 0.02$  eV are presented in Fig. 5(a) by the lines 1 and 2 for the band gap  $\Delta = 0.03$  and  $0.05$  eV, respectively. The vicinity of the points of minimum and maximum reflectance is shown on an enlarged scale in Fig. 5(b). As can be seen in these figures, the presence of a nonzero band gap leads to considerable changes as compared to the line 1 in Fig. 1 computed at the same temperature and chemical potential, but with  $\Delta = 0$ . The most important novel feature is that under the condition  $\hbar\omega = \Delta$  we have  $\text{Im}\sigma = \infty$  and, as a result,  $\mathcal{R} = 1$  [see Eqs. (7) and (10)]. The respective two peaks in Figs. 5(a) and 5(b) are unphysically narrow (this point is discussed in Ref. [47]). Another distinctive feature of the case  $\Delta \neq 0$  is that the minimum values of  $\mathcal{R}$  are reached exactly at the frequencies  $\omega_0$  where  $\text{Im}\sigma(\omega_0) = 0$ . In Fig. 5 we have  $\hbar\omega_0 = \hbar\omega_m = 0.0287$  eV for the line 1 and  $\hbar\omega_0 = \hbar\omega_m = 0.0375$  eV for the line 2. The respective minimum reflectance  $\mathcal{R}(\omega_m) = 0$  because for both lines the inequality  $\hbar\omega_m < \Delta$  is valid and, in accordance with Eq. (8), it holds  $\text{Re}\sigma(\omega_m) = 0$ . In the wide range of frequencies  $\hbar\omega < 0.01$  eV the reflectance of graphene increases with decreasing band gap.

We now turn our attention to the discussion of the role of varying temperature in the case of nonzero band gap. For this purpose, the lines 1 and 2 in Fig. 6 show the computational results for the reflectance of graphene with  $\mu = 0.02$  eV as a function of frequency for the band gap  $\Delta = 0.03$  and  $0.05$  eV, respectively, at (a)  $T = 77$  K and (b)  $T = 4.4$  K. As is seen in Figs. 6(a) and 6(b), under the condition  $\hbar\omega = \Delta$  the imaginary part of conductivity is infinitely large and  $\mathcal{R} = 1$ . Similar to the case of  $T = 300$  K in Fig. 5, this happens at  $\hbar\omega = 0.03$  eV for the line 1 and at  $\hbar\omega = 0.05$  eV for the line 2 in both Figs. 6(a) and 6(b). The position of the points of minimum  $\omega_m$ , contrastingly, depends on temperature. For the lines 1 and 2 in Fig. 6(a) ( $T = 77$  K), we have  $\hbar\omega_m = 0.019$  and  $0.014$  eV, respectively [we recall that here, again, the minimum value of reflectance is reached at  $\omega_m = \omega_0$  where

$\text{Im}\sigma(\omega_0) = 0$ ]. Taking into account that  $\hbar\omega_m < \Delta$ , Eq. (8) leads to  $\text{Re}\sigma(\omega_m) = 0$  and, thus,  $\mathcal{R}(\omega_m) = 0$ . In Fig. 6(b) ( $T = 4.4$  K),  $\hbar\omega_m = 0.014$  eV for the line 1. For the line 2 the minimum of reflectance is reached at a very small frequency. In both cases  $\text{Re}\sigma(\omega_m) = 0$  and  $\mathcal{R}(\omega_m) = 0$ . Comparing Figs. 5 and 6, one can conclude that with decreasing temperature the position of the points of minimum shifts to smaller frequencies. It should be noted also that there is a small peak on the line 1 in Fig. 6(b) at the frequency  $\hbar\omega = 2\mu = 0.04$  eV. It appears for the same reason as was explained above when discussing Fig. 2(b). In the case of gapped graphene this explanation is applicable only under the condition  $2\mu > \Delta$  satisfied for the line 1. For the line 2 in Fig. 6(b) it holds  $2\mu < \Delta$  and no additional peaks appear.

Some of the numerical results obtained above can be reproduced analytically using the asymptotic expressions presented in Sec. II. Thus, for the line 1 in Fig. 6(b) one has  $k_B T = 0.00038$  eV  $\ll \mu = 0.02$  eV and  $\Delta = 0.03$  eV  $< 2\mu = 0.04$  eV. Because of this, the asymptotic expression (12) should be applicable in this case at sufficiently low frequencies. In fact Eq. (7) for  $\mathcal{R}$  with  $\text{Re}\sigma = 0$  and  $\text{Im}\sigma$  given by Eq. (12) agrees with the results of numerical computations to within 1% at  $\hbar\omega < 0.01$  meV.

As one more example, we consider the line 2 in Fig. 6(b). Here, again,  $k_B T \ll \mu = 0.02$  eV, but  $\Delta = 0.05$  eV  $> 2\mu$ . Because of this, the asymptotic expression (13) is applicable. One can check that the substitution of Eq. (13) in Eq. (7) leads to the values of  $\mathcal{R}$  in agreement to within 1% with the results of numerical computations in the wide frequency regions  $\hbar\omega < 5 \times 10^{-11}$  eV and  $0.2$  meV  $< \hbar\omega < 0.05$  eV (we recall that for these frequencies  $\text{Re}\sigma$  is again equal to zero).

The asymptotic expression (13) also allows to estimate the value of frequency where the reflectance of graphene vanishes:  $\mathcal{R}(\omega_m) = 0$ . In this case  $\omega_m = \omega_0$  where  $\text{Im}\sigma(\omega_0) = 0$ . Taking into account that for the line 2 we have  $\hbar\omega_0 \ll \Delta$  [in Fig. 6(b) the region of so low frequencies is not shown], one can expand in Eq. (13) up to the first power in the small parameter  $\hbar\omega/\Delta$  and obtain

$$\text{Im}\sigma(\omega) \approx \frac{\sigma_0}{\pi} \left( -\frac{8}{3} \frac{\hbar\omega}{\Delta} + \frac{16k_B T}{\hbar\omega} e^{-\frac{\Delta}{2k_B T}} \cosh \frac{\mu}{k_B T} \right). \quad (22)$$

The root of this expression is equal to

$$\hbar\omega_0 = \left( 6k_B T \Delta e^{-\frac{\Delta}{2k_B T}} \cosh \frac{\mu}{k_B T} \right)^{1/2}. \quad (23)$$

For the values all the parameters under consideration this results in  $\hbar\omega_0 \approx 0.01$  meV. Although in a vicinity of the point of minimum  $\mathcal{R}$  the asymptotic expression is not as exact,

as in the frequency regions indicated above, the obtained value is in qualitative agreement with  $\hbar\omega_0 = 0.015$  meV found by means of numerical computations.

In the end of this section we consider the dependence of  $\mathcal{R}$  on the chemical potential for the gapped graphene at different temperatures. In Fig. 7 the computational results are presented for the reflectance of graphene with  $\Delta = 0.1$  eV at the frequency  $\hbar\omega = 0.01$  eV as a function of  $\mu$ . The lines 1, 2, and 3 are plotted at  $T = 300, 77,$  and  $4.4$  K, respectively. As is seen in Fig. 7, the lines 2 and 3 reach their minimum values at  $\mu = 0.035$  and  $0.0506$  eV, respectively. For these values of  $\mu$  it holds  $\text{Im}\sigma(0.01 \text{ eV}/\hbar) = 0$  at  $T = 77$  and  $4.4$  K, respectively. Taking into account also that  $\hbar\omega = 0.01 \text{ eV} < \Delta$ , one concludes that  $\text{Re}\sigma = 0$  and, thus,  $\mathcal{R} = 0$ . From the comparison of Figs. 7 and 3, we find that the presence of a nonzero band gap results in a considerable decrease of graphene reflectance.

The obtained results strongly depend on the specific values of frequency and band gap. In Fig. 8(a) the reflectance of gapped graphene with  $\Delta = 0.1$  eV (the same as in Fig. 7), but at the frequency  $\hbar\omega = 0.07$  eV, is plotted as a function of  $\mu$  by the lines 1, 2, and 3 at  $T = 300, 77,$  and  $4.4$  K, respectively. In this case all the three lines are of the same character, and the lines 2 and 3 are almost coinciding. In the region  $2\mu < \Delta = 0.1$  eV at  $T = 77$  and  $4.4$  K the reflectance is nearly independent on  $\mu$ . The minimum values of  $\mathcal{R}$  on the lines 1, 2, and 3 are reached at  $\mu = 0.0726, 0.0791,$  and  $0.0787$ , respectively. For these values of  $\mu$  we have  $\text{Im}\sigma(0.07 \text{ eV}/\hbar) = 0$  at  $T = 300, 77,$  and  $4.4$  K, respectively. The minimum reflectance vanishes,  $\mathcal{R} = 0$ , because  $\hbar\omega = 0.07 \text{ eV} < \Delta$  and, thus,  $\text{Re}\sigma(\omega) = 0$ .

Note that in Figs. 5–7 and 8(a) plotted for a gapped graphene the minimum reflectance is  $\mathcal{R} = 0$ . This means that in the narrow vicinities of points, where the minimum is reached, one cannot use Eq. (15) for calculation of the angular dependence of the TM and TE reflectances. For this purpose the nonlocal corrections to the conductivity of graphene would be required. Equation (15), however, still stands over the entire region of frequencies with exception of only narrow vicinities of the points of minimum reflectance.

Finally, in Fig. 8(b) we plot the reflectance of gapped graphene with  $\Delta = 0.04$  eV at  $\hbar\omega = 0.07$  eV as a function of  $\mu$ . The three lines 1, 2, and 3 are again plotted at  $T = 300, 77,$  and  $4.4$  K, respectively. All the three lines in Fig. 8(b) differ qualitatively. Unlike the previous figure, now  $\hbar\omega > \Delta$  which means that  $\text{Re}\sigma \neq 0$  [see Eq. (8)]. As a result, the minimum values of  $\mathcal{R}$  are not equal to zero, but are determined by the value of  $\text{Re}\sigma(0.07 \text{ eV}/\hbar)$ . [We recall that at the point of minimum  $\text{Im}\sigma(0.07 \text{ eV}/\hbar) = 0$ .] At  $T = 300,$

77, and 4.4 K, i.e., for the lines 1, 2, and 3, the respective minimum values of  $\mathcal{R}$  are equal to  $4.8 \times 10^{-5}$ ,  $4.5 \times 10^{-6}$ , and  $1.2 \times 10^{-11}$ . They are reached at  $\mu = 0.044$ ,  $0.048$ , and  $0.04455$  eV, respectively. A small peak on the line 3 ( $T = 4.4$  K) arises at  $\mu = \hbar\omega/2 = 0.035$  eV for the reasons discussed above.

## V. CONCLUSIONS AND DISCUSSION

In the foregoing, we have investigated the impact of chemical potential on the reflectance of graphene in the application region of the Dirac model, i.e., in the microwave and infrared domains. For this purpose, the reflectance was expressed via the polarization tensor or, alternatively, via the conductivity of graphene. Both these quantities have been found recently for arbitrary values of the chemical potentials and band-gap parameter at any temperature in the framework of the Dirac model basing on the first principles of quantum electrodynamics.

The obtained expressions were used to perform numerical computations of the graphene reflectance at the normal incidence as a function of frequency and chemical potential at different temperatures. Both the cases of gapless and gapped graphene were considered. It is shown that the major impact of chemical potential on the graphene reflectance occurs in the domain of infrared optics. In this domain the reflectance possesses the minimum values reached at the roots of the imaginary part of the conductivity of graphene. The magnitudes of the minimum values of reflectance are either equal to zero or determined by the real part of conductivity if the latter is nonzero. The reflectance of gapped graphene is lower than that of a gapless one. Over the wide range of frequencies, the reflectance of graphene increases with increasing chemical potential and decreasing band gap. We have also demonstrated that the reflectance of gapped graphene possesses narrow peaks and turns to unity at the frequencies where the imaginary part of conductivity turns to infinity. By and large the reflectance of graphene is determined by the values of frequency, temperature, band-gap parameter, chemical potential and their interplay. The results of numerical computations and analytic asymptotic calculations were compared and found to be in good agreement. At higher frequencies and, specifically, for visible light, some theoretical approaches beyond the scope of the Dirac model are developed (see Sec. I and, e.g., Refs. [59–61] where small quadratic in momentum subdominant contributions to a dominant linear Dirac Hamiltonian

are considered).

To conclude, the developed complete theory of the reflectance of graphene takes into account the combined effect of its realistic properties, such as nonzero chemical potential and band-gap parameter in the application region of the Dirac model. The obtained results could be interesting not only for fundamental physics, but for the listed above numerous technological applications of graphene.

### Acknowledgments

The work of V.M.M. was partially supported by the Russian Government Program of Competitive Growth of Kazan Federal University.

- 
- [1] M. I. Katsnelson, *Graphene: Carbon in Two Dimensions* (Cambridge University Press, Cambridge, 2012).
  - [2] *Physics of Graphene*, ed. H. Aoki and M. S. Dresselhaus (Springer, Cham, 2014).
  - [3] V. P. Gusynin, S. G. Sharapov, and J. P. Carbotte, AC conductivity of graphene: From tight-binding model to 2+1-dimensional quantum electrodynamics, *Int. J. Mod. Phys. B* **21**, 4611 (2007).
  - [4] N. M. R. Peres, The transport properties of graphene: An introduction, *Rev. Mod. Phys.* **82**, 2673 (2010).
  - [5] S. Das Sarma, S. Adam, E. H. Hwang, and E. Rossi, Electronic transport in two-dimensional graphene, *Rev. Mod. Phys.* **83**, 407 (2011).
  - [6] L. A. Falkovsky and S. S. Pershoguba, Optical far-infrared properties of a graphene monolayer and multilayer, *Phys. Rev. B* **76**, 153410 (2007).
  - [7] T. Stauber, N. M. R. Peres, and A. K. Geim, Optical conductivity of graphene in the visible region of the spectrum, *Phys. Rev. B* **78**, 085432 (2008).
  - [8] K. F. Mak, M. Y. Sfeir, Y. Wu, C. H. Lui, J. A. Misewich, and T. F. Heinz, Measurement of the optical conductivity of graphene, *Phys. Rev. Lett.* **101**, 196405 (2008).
  - [9] L. A. Falkovsky, Optical properties of graphene, *J. Phys.: Conf. Series* **129**, 012004 (2008).
  - [10] J. M. Dawlaty, S. Shivaraman, J. Strait, P. George, Mvs. Chandrasheknar, F. Rana, M. G.

- Spencer, D. Veksler, and Y. Chen, Measurement of the optical absorption spectra of epitaxial graphene from terahertz to visible, *Appl. Phys. Lett.* **93**, 131905 (2008).
- [11] B. Sensale-Rodriguez, R. Yan, S. Rafique, M. Zhu, W. Li, X. Liang, D. Gundlach, V. Protasenko, M. M. Kelly, D. Jena, L. Liu, and H. G. Xing, Extraordinary control of terahertz beam reflectance in graphene electro-absorption modulators, *Nano Lett.* **12**, 4518 (2012).
- [12] L. M. Malard, K. F. Mak, A. H. Castro-Neto, N. M. R. Peres, and T. F. Heinz, Observation of intra- and inter-band transitions in the transient optical response of graphene, *New J. Phys.* **15**, 015009 (2013).
- [13] C. N. Santos, F. Joucken, D. De Sousa Meneses, P. Echegut, J. Campos-Delgado, P. Louette, J.-P. Raskin, and B. Haskens, Terahertz and mid-infrared reflectance of epitaxial graphene, *Scient. Rep.* **6**, 24301 (2016).
- [14] Yu. V. Bludov, M. I. Vasilevskiy, and N. M. R. Peres, Mechanism for graphene-based optoelectronic switches by turning surface plasmon-polariton in monolayer graphene, *Europhys. Lett.* **92**, 68001 (2010).
- [15] W. Hong, Yu. Xu, G. Lu, Ch. Li, and G. Shi, Transparent graphene/PEDOT-PSS composite films as counter electrodes of dye-sensitized solar cells, *Electrochem. Commun.* **10**, 1555 (2008).
- [16] L. F. Dumée, L. He, Z. Wang, P. Sheath, J. Xiong, C. Feng, M. Y. Tan, F. She, M. Duke, S. Gray, A. Pacheco, P. Hodgson, M. Majumder, and L. Kong, Growth of nano-textured graphene coatings across highly porous stainless steel supports towards corrosion resistant coatings, *Carbon* **87**, 395 (2015).
- [17] S. Watcharotone, D. A. Dikin, S. Stankovich, R. Piner, I. Jung, G. H. B. Dommett, G. Evmenenko, S.-E. Wu, S.-F. Chen, C.-P. Liu, S. T. Nguyen, and R. S. Ruoff, Graphene-silica composite thin films as transparent conductors, *Nano Lett.* **7**, 1888 (2007).
- [18] A. H. Castro Neto, F. Guinea, N. M. R. Peres, K. S. Novoselov, and A. K. Geim, The electronic properties of graphene, *Rev. Mod. Phys.* **81**, 109 (2009).
- [19] T. Stauber, J. Schliemann, and N. M. R. Peres, Dynamical polarizability of graphene beyond the Dirac cone approximation, *Phys. Rev. B* **81**, 085409 (2010).
- [20] Zhou Li and J. P. Carbotte, Longitudinal and spin-valley Hall optical conductivity in single layer MoS<sub>2</sub>, *Phys. Rev. B* **86**, 205425 (2012).
- [21] Zhou Li and J. P. Carbotte, Phonon structure in dispersion curves and density of states of

- massive Dirac fermions, *Phys. Rev. B* **88**, 045417 (2013).
- [22] Zhou Li and J. P. Carbotte, Impact of electron-phonon interaction on dynamic conductivity of gapped Dirac fermions: Application to single layer MoS<sub>2</sub>, *Physica B: Condensed Matter* **421**, 97 (2013).
- [23] Zhou Li and J. P. Carbotte, Conductivity of Dirac fermions with phonon-induced topological crossover, *Phys. Rev. B* **88**, 195133 (2013).
- [24] N. Yu. Astrakhantsev, V. V. Braguta, and M. I. Katsnelson, Many-body effects in graphene beyond the Dirac model with Coulomb interaction, *Phys. Rev. B* **92**, 245105 (2015).
- [25] M. Bordag, I. V. Fialkovsky, D. M. Gitman, and D. V. Vassilevich, Casimir interaction between a perfect conductor and graphene described by the Dirac model, *Phys. Rev. B* **80**, 245406 (2009).
- [26] P. K. Pyatkovsky, Dynamical polarization, screening, and plasmons in gapped graphene, *J. Phys.: Condens. Matter* **21**, 025506 (2009).
- [27] I. V. Fialkovsky, V. N. Marachevsky, and D. V. Vassilevich, Finite-temperature Casimir effect for graphene, *Phys. Rev. B* **84**, 035446 (2011).
- [28] M. Bordag, G. L. Klimchitskaya, and V. M. Mostepanenko, Thermal Casimir effect in the interaction of graphene with dielectrics and metals, *Phys. Rev. B* **86**, 165429 (2012).
- [29] M. Chaichian, G. L. Klimchitskaya, V. M. Mostepanenko, and A. Tureanu, Thermal Casimir-Polder interaction of different atoms with graphene, *Phys. Rev. A* **86**, 012515 (2012).
- [30] G. L. Klimchitskaya and V. M. Mostepanenko, Van der Waals and Casimir interactions between two graphene sheets, *Phys. Rev. B* **87**, 075439 (2013).
- [31] B. Arora, H. Kaur, and B. K. Sahoo,  $C_3$  coefficients for the alkali atoms interacting with a graphene and carbon nanotube, *J. Phys. B* **47**, 155002 (2014).
- [32] K. Kaur, J. Kaur, B. Arora, and B. K. Sahoo, Emending thermal dispersion interaction of Li, Na, K and Rb alkali-metal atoms with graphene in the Dirac model, *Phys. Rev. B* **90**, 245405 (2014).
- [33] G. L. Klimchitskaya and V. M. Mostepanenko, Classical Casimir-Polder force between polarizable microparticles and thin films including graphene, *Phys. Rev. A* **89**, 012516 (2014).
- [34] G. L. Klimchitskaya and V. M. Mostepanenko, Classical limit of the Casimir interaction for thin films with applications to graphene, *Phys. Rev. B* **89**, 035407 (2014).
- [35] G. L. Klimchitskaya and V. M. Mostepanenko, Observability of thermal effects in the Casimir

- interaction from graphene-coated substrates, *Phys. Rev. A* **89**, 052512 (2014).
- [36] G. L. Klimchitskaya and V. M. Mostepanenko, Impact of graphene coating on the atom-plate interaction, *Phys. Rev. A* **89**, 062508 (2014).
- [37] G. L. Klimchitskaya, V. M. Mostepanenko, and Bo E. Sernelius, Two approaches for describing the Casimir interaction with graphene: density-density correlation function versus polarization tensor, *Phys. Rev. B* **89**, 125407 (2014).
- [38] G. L. Klimchitskaya, U. Mohideen, and V. M. Mostepanenko, Theory of the Casimir interaction for graphene-coated substrates using the polarization tensor and comparison with experiment, *Phys. Rev. B* **89**, 115419 (2014).
- [39] M. Bordag, G. L. Klimchitskaya, V. M. Mostepanenko, and V. M. Petrov, Quantum field theoretical description for the reflectivity of graphene, *Phys. Rev. D* **91**, 045037 (2015); **93**, 089907(E) (2016).
- [40] G. L. Klimchitskaya and V. M. Mostepanenko, Origin of large thermal effect in the Casimir interaction between two graphene sheets, *Phys. Rev. B* **91**, 174501 (2015).
- [41] G. L. Klimchitskaya, Quantum field theory of the Casimir force for graphene, *Int. J. Mod. Phys. A* **31**, 1641026 (2016).
- [42] V. B. Bezerra, G. L. Klimchitskaya, V. M. Mostepanenko, and C. Romero, Nernst heat theorem for the thermal Casimir interaction between two graphene sheets, *Phys. Rev. A* **94**, 042501 (2016).
- [43] G. Bimonte, G. L. Klimchitskaya, and V. M. Mostepanenko, How to observe the giant thermal effect in the Casimir force for graphene systems, *Phys. Rev. A* **96**, 012517 (2017).
- [44] G. L. Klimchitskaya and V. M. Mostepanenko, Conductivity of pure graphene: Theoretical approach using the polarization tensor, *Phys. Rev. B* **93**, 245419 (2016).
- [45] G. L. Klimchitskaya and V. M. Mostepanenko, Quantum electrodynamic approach to the conductivity of gapped graphene, *Phys. Rev. B* **94**, 195405 (2016).
- [46] G. L. Klimchitskaya, C. C. Korikov, and V. M. Petrov, Theory of reflectivity properties of graphene-coated material plates, *Phys. Rev. B* **92**, 125419 (2015); **93**, 159906(E) (2016).
- [47] G. L. Klimchitskaya and V. M. Mostepanenko, Reflectivity properties of graphene with nonzero mass-gap parameter, *Phys. Rev. A* **93**, 052106 (2016).
- [48] G. L. Klimchitskaya and V. M. Mostepanenko, Optical properties of dielectric plates coated with gapped graphene, *Phys. Rev. B* **95**, 035425 (2017).

- [49] M. Bordag, I. Fialkovskiy, and D. Vassilevich, Enhanced Casimir effect for doped graphene, *Phys. Rev. B* **93**, 075414 (2016); **95**, 119905(E) (2017).
- [50] G. Bimonte, G. L. Klimchitskaya, and V. M. Mostepanenko, Thermal effect in the Casimir force for graphene and graphene-coated substrates: Impact of nonzero mass gap and chemical potential, *Phys. Rev. B* **96**, 115430 (2017).
- [51] C. Henkel, G. L. Klimchitskaya, and V. M. Mostepanenko, Influence of chemical potential on the Casimir-Polder interaction between an atom and gapped graphene or graphene-coated substrate, *Phys. Rev. A* **97**, 032504 (2018).
- [52] G. L. Klimchitskaya, V. M. Mostepanenko, and V. M. Petrov, Conductivity of graphene in the framework of Dirac model: Interplay between nonzero mass gap and chemical potential, *Phys. Rev. B* **96**, 235432 (2017).
- [53] G. L. Klimchitskaya and V. M. Mostepanenko, Kramers-Kronig relations and causality conditions for graphene in the framework of the Dirac model, *Phys. Rev. D* **97**, 085001 (2018).
- [54] D. Liu and S. Zhang, Kramers-Kronig relation of graphene conductivity, *J. Phys.: Condens. Matter* **20**, 175222 (2008).
- [55] M. Jablan, H. Buljan, and M. Soljačić, Transverse electric plasmons in bilayer graphene, *Optics Express* **19**, 11236 (2011).
- [56] J. Horng, Chi-Fan Chen, B. Geng, C. Girit, Y. Zhang, Z. Hao, H. A. Bechtel, M. Martin, A. Zettl, M. F. Crommie, Y. R. Shen, and F. Wang, Drude conductivity of Dirac fermions in graphene, *Phys. Rev. B* **83**, 165113 (2011).
- [57] V. U. Nazarov, Negative static permittivity and violation of Kramers-Kronig relations in quasi-two-dimensional crystals, *Phys. Rev. B* **92**, 161402(R) (2015).
- [58] M. Bordag, G. L. Klimchitskaya, U. Mohideen, and V. M. Mostepanenko, *Advances in the Casimir Effect* (Oxford University Press, Oxford, 2015).
- [59] Zhou Li and J. P. Carbotte, Magneto-optical conductivity in a topological insulator, *Phys. Rev. B* **88**, 045414 (2013).
- [60] Zhou Li and J. P. Carbotte, Particle-hole asymmetry on Hall conductivity of a topological insulator, *Phys. Rev. B* **89**, 085413 (2014).
- [61] Zhou Li and J. P. Carbotte, Optical spectral weight: Comparison of weak and strong spin-orbit coupling, *Phys. Rev. B* **91**, 115421 (2015).

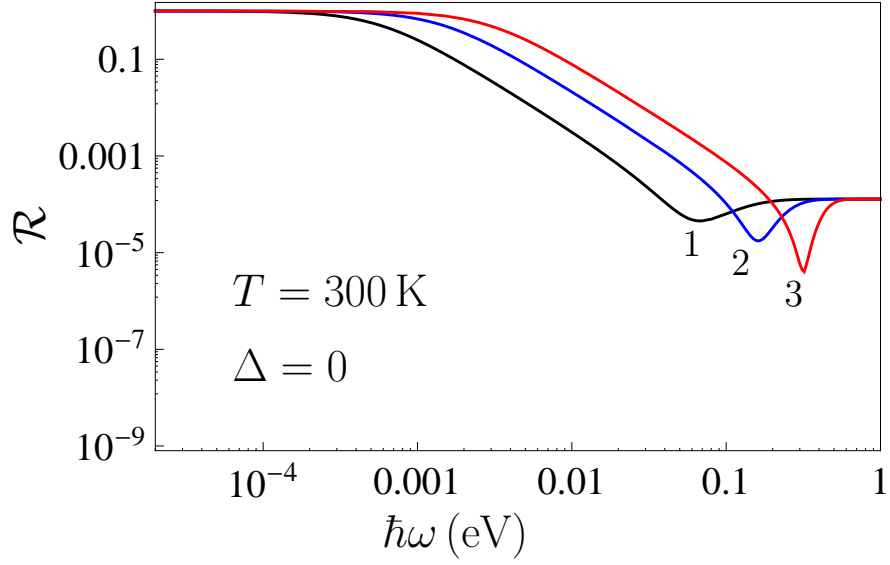


FIG. 1: The reflectance of gapless graphene at  $T = 300 \text{ K}$  is shown as a function of frequency by the lines 1, 2, and 3 for the chemical potential  $\mu = 0.02, 0.1, \text{ and } 0.2 \text{ eV}$ , respectively.

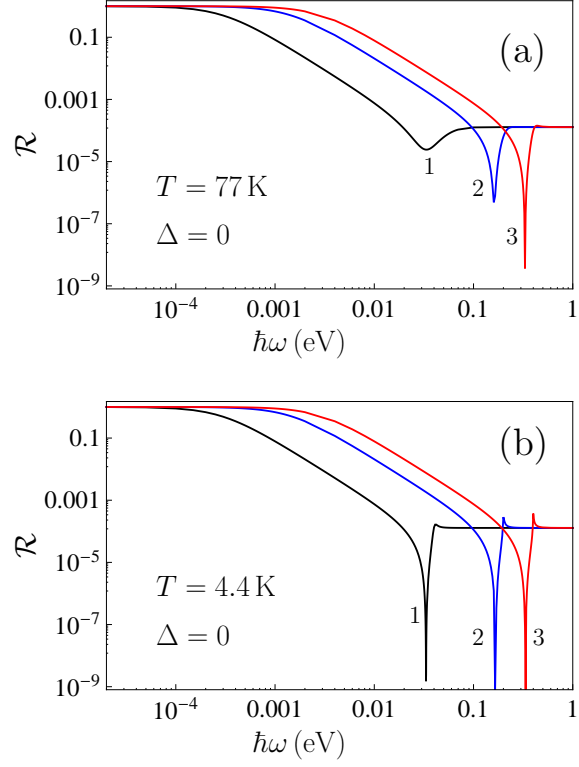


FIG. 2: The reflectance of gapless graphene at (a)  $T = 77$  K and (b)  $T = 4.4$  K is shown as a function of frequency by the lines 1, 2, and 3 for the chemical potential  $\mu = 0.02, 0.1,$  and  $0.2$  eV, respectively.

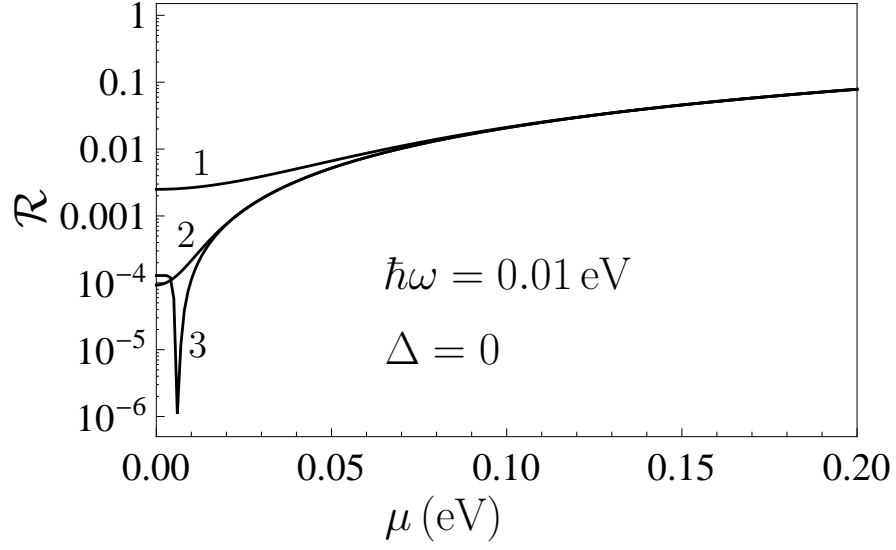


FIG. 3: The reflectance of gapless graphene at  $\hbar\omega = 0.01 \text{ eV}$  is shown as a function of the chemical potential by the lines 1, 2, and 3 at  $T = 300, 77,$  and  $4.4 \text{ K}$ , respectively.

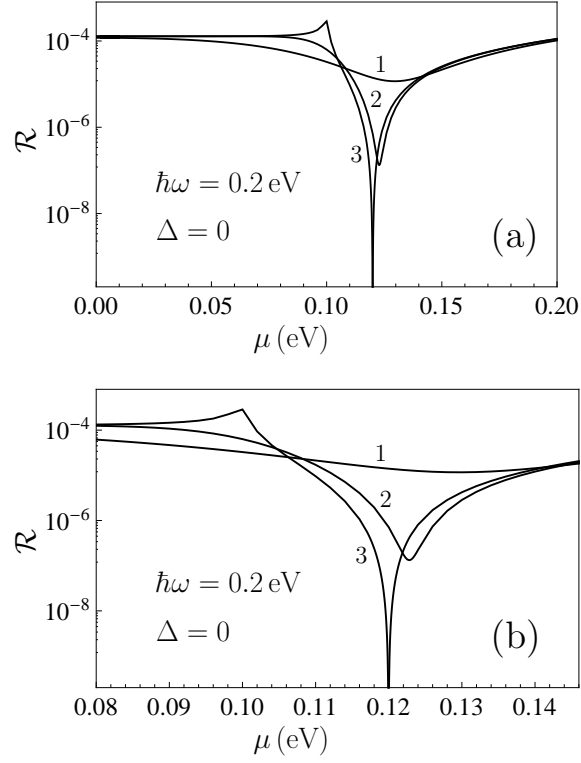


FIG. 4: (a) The reflectance of gapless graphene at  $\hbar\omega = 0.2$  eV is shown as a function of the chemical potential by the lines 1, 2, and 3 at  $T = 300$ ,  $77$ , and  $4.4$  K, respectively. (b) A vicinity of the points of minimum reflectance is shown on an enlarged scale.

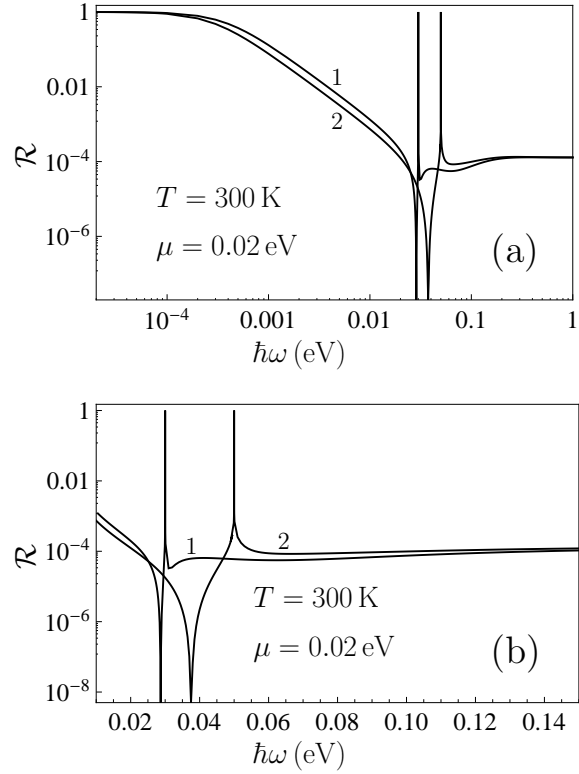


FIG. 5: (a) The reflectance of gapped graphene with  $\mu = 0.02$  eV at  $T = 300$  K is shown as a function of frequency by the lines 1 and 2 for the band gap  $\Delta = 0.03$  and  $0.05$  eV, respectively. (b) A vicinity of the points of minimum reflectance is shown on an enlarged scale.

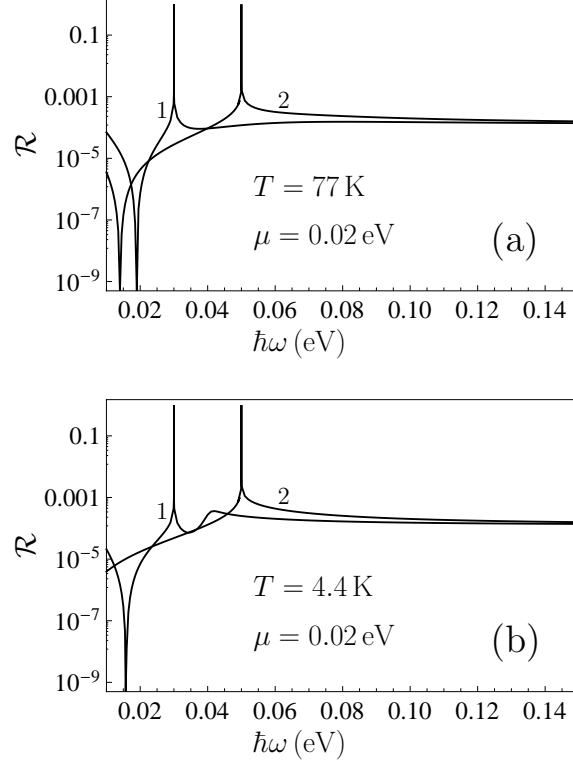


FIG. 6: The reflectance of gapped graphene with  $\mu = 0.02$  eV at (a)  $T = 77$  K and (b)  $T = 4.4$  K is shown as a function of frequency by the lines 1 and 2 for the band gap  $\Delta = 0.03$  and  $0.05$  eV, respectively.

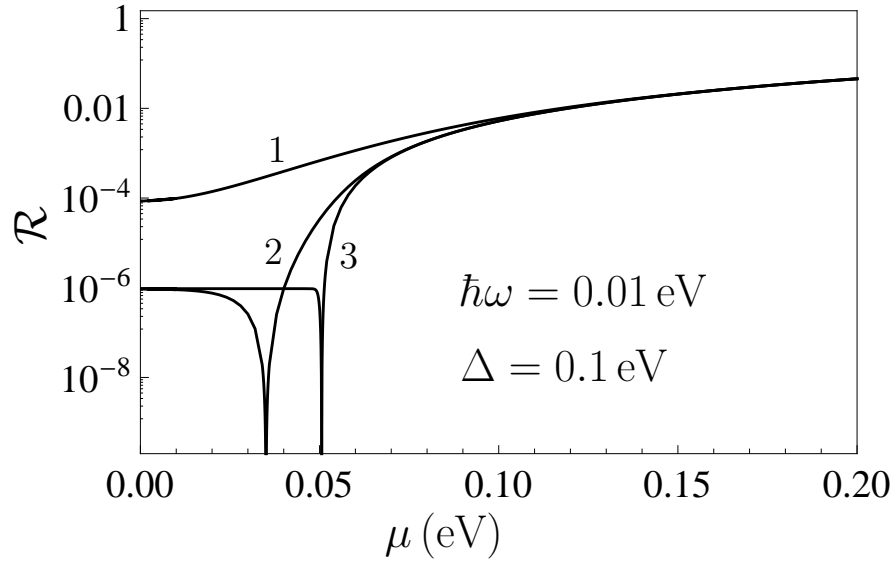


FIG. 7: The reflectance of gapped graphene with  $\Delta = 0.1$  eV at  $\hbar\omega = 0.01$  eV is shown as a function of the chemical potential by the lines 1, 2, and 3 at  $T = 300$ , 77, and 4.4 K, respectively.

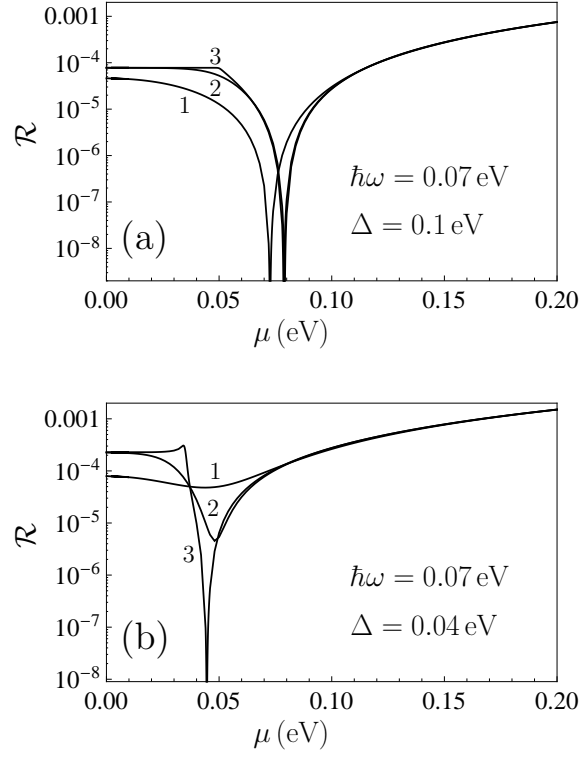


FIG. 8: The reflectance of gapped graphene with (a)  $\Delta = 0.1$  eV and (b)  $\Delta = 0.04$  eV at  $\hbar\omega = 0.07$  eV is shown as a function of the chemical potential by the lines 1, 2, and 3 at  $T = 300$ , 77, and 4.4 K, respectively.